



Hay, R. F., Gibson, G. M., Lee, M. P., Padgett, M. J., and Phillips, D. B. (2014) *Four-directional stereo-microscopy for 3D particle tracking with real-time error evaluation*. *Optics Express*, 22 (15). pp. 18662-18667. ISSN 1094-4087.

Copyright © 2014 Optical Society of America

<http://eprints.gla.ac.uk/95386/>

Deposited on: 30 July 2014

Four-directional stereo-microscopy for 3D particle tracking with real-time error evaluation

R. F. Hay,* G. M. Gibson, M. P. Lee, M. J. Padgett, and D. B. Phillips

SUPA, School of Physics and Astronomy, University of Glasgow, Glasgow, G12 8QQ, UK

[*r.hay.1@research.gla.ac.uk](mailto:r.hay.1@research.gla.ac.uk)

Abstract: High-speed video stereo-microscopy relies on illumination from two distinct angles to create two views of a sample from different directions. The 3D trajectory of a microscopic object can then be reconstructed using parallax to combine 2D measurements of its position in each image. In this work, we evaluate the accuracy of 3D particle tracking using this technique, by extending the number of views from two to four directions. This allows us to record two independent sets of measurements of the 3D coordinates of tracked objects, and comparison of these enables measurement and minimisation of the tracking error in all dimensions. We demonstrate the method by tracking the motion of an optically trapped micro-sphere of 5 μm in diameter, and find an accuracy of 2-5 nm laterally, and 5-10 nm axially, representing a relative error of less than 2.5% of its range of motion in each dimension.

© 2014 Optical Society of America

OCIS codes: (140.7010) Laser trapping; (170.4520) Optical confinement and manipulation; (350.4855) Optical tweezers or optical manipulation.

References and links

1. V. J. Anderson and H. N. W. Lekkerkerker, "Insights into phase transition kinetics from colloid science," *Nature* **416**, 811–815 (2002).
2. A. D. Mehta, M. Rief, J. A. Spudich, D. A. Smith, and R. M. Simmons, "Single-molecule biomechanics with optical methods," *Science* **283**, 1689–1695 (1999).
3. P. Cicuta and A. M. Donald, "Microrheology: a review of the method and applications," *Soft Matter* **3**(12), 1449–1455 (2007).
4. A. Rohrbach, C. Tischer, D. Neumayer, E.-L. Florin, and E. H. K. Stelzer, "Trapping and tracking a local probe with a photonic force microscope," *Rev. Sci. Instrum.* **75**(6), 2197–2210 (2004).
5. W. Xu, M. H. Jericho, H. J. Kreuzer, and I. A. Meinertzhagen, "Tracking particles in four dimensions with in-line holographic microscopy," *Opt. Lett.* **28**, 164–166 (2003).
6. Z. Zhang and C.-H. Menq, "Three-dimensional particle tracking with subnanometer resolution using off-focus images," *Appl. Opt.* **47**, 2361–2370 (2008).
7. J. S. Dam, I. R. Perch-Nielsen, D. Palima, and J. Glückstad, "Three-dimensional imaging in three-dimensional optical multi-beam micromanipulation," *Opt. Express* **16**(10), 7244–7250 (2008).
8. J. S. Dam, I. Perch-Nielsen, D. Palima, and J. Glückstad, "Multi-particle three-dimensional coordinate estimation in real-time optical manipulation," *J. Eur. Opt. Soc. Rapid Publ.* **4**, 09045 (2009).
9. R. Bowman, G. Gibson, and M. Padgett, "Particle tracking stereomicroscopy in optical tweezers: Control of trap shape," *Opt. Express* **18**(11), 11785–11790 (2010).
10. R. Bowman, D. Preece, G. Gibson, and M. Padgett, "Stereoscopic particle tracking for 3D touch, vision and closed-loop control in optical tweezers," *J. Opt.* **13**(4), 044003 (2011).
11. D. B. Phillips, G. M. Gibson, R. Bowman, M. J. Padgett, S. Hanna, D. M. Carberry, M. J. Miles, and S. H. Simpson, "An optically actuated surface scanning probe," *Opt. Express* **20**, 29679–29693 (2012).
12. C. Alpmann, R. Bowman, M. Woerdemann, M. Padgett, and C. Denz, "Mathieu beams as versatile light moulds for 3d micro particle assemblies," *Opt. Express* **18**, 26084–26091 (2010).

13. S. N. Olof, J. A. Grieve, D. B. Phillips, H. Rosenkranz, M. L. Yallop, M. J. Miles, A. J. Patil, S. Mann, and D. M. Carberry, "Measuring nanoscale forces with living probes," *Nano Lett.* **12**, 6018–6023 (2012).
14. D. B. Phillips, S. H. Simpson, J. A. Grieve, R. Bowman, G. M. Gibson, M. J. Padgett, J. Rarity, S. Hanna, M. J. Miles, and D. Carberry, "Force sensing with a shaped dielectric micro-tool," *Europhys. Lett.* **99**, 58004 (2012).
15. D. B. Phillips, M. J. Padgett, S. Hanna, Y.-L. Ho, D. M. Carberry, M. J. Miles, and S. H. Simpson, "Shape-induced force fields in optical trapping," *Nat. Photon.* **8**, 400–405 (2014).
16. M. Hasler, T. Haist, and W. Osten, "Stereo vision in spatial-light-modulator-based microscopy," *Opt. Lett.* **37**, 2238–2240 (2012).
17. C. Maurer, A. Jesacher, S. Bernet, and M. Ritsch-Marte, "What spatial light modulators can do for optical microscopy," *Laser Photon. Rev.* **5**, 81–101 (2011).
18. M. P. Lee, G. M. Gibson, R. Bowman, S. Bernet, M. Ritsch-Marte, D. B. Phillips, and M. J. Padgett, "A multi-modal stereo microscope based on a spatial light modulator," *Opt. Express* **21**(14), 16541–16551 (2013).
19. M. P. Lee, G. M. Gibson, D. Phillips, M. J. Padgett, and M. Tassieri, "Dynamic stereo microscopy for studying particle sedimentation," *Opt. Express* **22**, 4671–4677 (2014).
20. F. Saglimbeni, S. Bianchi, A. Lepore, and R. Di Leonardo, "Three-axis digital holographic microscopy for high speed volumetric imaging," *Opt. Express* **22**(11), 13710–13718 (2014).
21. O. Otto, F. Czerwinski, J. L. Gornall, G. Stober, L. B. Oddershede, R. Seidel, and U. F. Keyser, "Real-time particle tracking at 10,000 fps using optical fiber illumination," *Opt. Express* **18**(22), 22722–22733 (2010).

1. Introduction

High-resolution measurement of the three-dimensional trajectories of microscopic objects is important in a wide range of fields from colloid science to biophysics [1, 2]. It is often used in conjunction with optical tweezers, where the motion of optically trapped objects can be used to recover a wealth of detailed information about their surroundings [3]. A variety of techniques have been developed to achieve three dimensional tracking, such as using a quadrant photodiode to observe the interference pattern generated in a laser beam as it is focussed through a sample [4], digital holographic microscopy [5], image correlation [6] and stereo-microscopy [7]. Each of these is suited to particular applications, but in all cases it is important to quantify the quality of the tracking in terms of its accuracy.

A stereo-microscope enables three dimensional visualisation of a sample by providing two views of it from different directions. An object that moves axially in the sample is observed to move laterally in each image by an amount and direction that is dependent upon the viewing angle. By illuminating from two distinct directions simultaneously, two views of the sample from different angles can be imaged using a single objective lens [7]. The superimposed images can be separated by channel colour [8], or by redirecting the light in the Fourier plane of the sample with a bi-prism [9]. By performing two dimensional tracking of the position of a particle in each image, its three dimensional coordinates can be reconstructed using parallax. High-speed video stereo-microscopy has been used in a variety of situations, including the axial position clamping of optically trapped objects [10, 11], the observation of optically stacked particles [12], tracking of live algae and artificial non-spherical structures [13, 14], and in an optically controlled scanning probe microscope [15].

The functionality of stereo-microscopy has been further expanded by replacing the bi-prism with a spatial light modulator (SLM) [16, 17]. The SLM separates the images by diffracting the light from each illumination direction to a different position on the camera. The flexibility of an SLM enables the incorporation of stereo-scopic imaging with additional modalities such as dark-field imaging [18] and dynamic refocussing to track particles over an increased depth of field [19]. A stereo-scopic version of digital holography has also recently been demonstrated, improving the axial resolution of holographic images [20].

In this work we demonstrate a stereo-microscope with four viewing directions, therefore providing two independent measurements of the 3D position of an optically trapped microsphere. Comparison of these measurements yields an estimate of the accuracy of the tracking in each dimension, in real-time. Previous work has provided an estimate of the accuracy in a

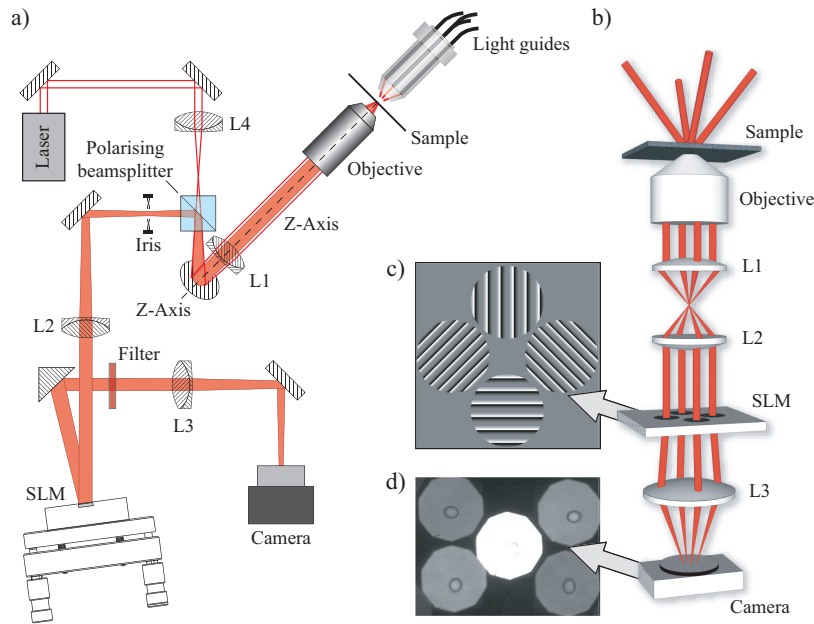


Fig. 1. a) Schematic of the optical layout. It is based on a transmission light microscope with an SLM placed in the Fourier plane of the image. The sample is illuminated from four directions with red LEDs (Luxeon Rebel, peak emission at 636 nm) coupled into light guides. Light transmitted through the sample is collected by the objective lens (Zeiss Plan-Neofluar, 100 \times , 1.3 NA). The polarising beamsplitter selects light of the correct polarisation for the SLM. An iris in a conjugate image plane controls the field-of-view to ensure all images fit adjacently onto the camera. A narrowband filter (635 nm / 10 nm) minimises dispersion of the images when diffracted from the SLM. The polarising beamsplitter is also used to couple in a single beam optical tweezer ($\lambda = 635$ nm). The focal lengths of the lenses are: L1 = 120 mm, L2 = 150 mm and L3 = 200 mm. b) Illustration of the four illumination paths through the system. Here the SLM is shown as a transmissive element rather than reflective, for clarity. The SLM diffracts light corresponding to each illumination direction to a separate region of the camera sensor. (c) A representative phase pattern on the SLM. (d) The resulting image on the camera. Undiffracted zero-order light is sent to the central region. The scaling is 73.5 nm per pixel.

single lateral dimension [10] or the noise on a static object (i.e. the precision or repeatability of the technique) [18], but our goal here is to measure the accuracy of axial tracking of an optically trapped object while it is undergoing Brownian motion, as this is representative of the situation in which the technique is most often used. We investigate how tracking errors depend on the degree of spatial filtering and exposure time of each image, and optimise the system.

2. Methods

2.1. Experimental set-up

Figure 1 shows a schematic of the experimental set-up. We use a compact design for stability, based on the microscope described by Lee et al. [19], with a modified illuminator which holds four optical fibre light guides each illuminating the sample from a different direction. We use an SLM to diffract each of the four views of the sample to a different location on the camera. The optical layout is shown in Fig. 1(a), and the four illumination paths through the system are

shown in Fig. 1(b). Each illumination direction corresponds to a unique position in the Fourier plane of the sample where the SLM is positioned. The pattern displayed on the SLM is shown in Fig. 1(c), it consists of four apertures, each centred on a position corresponding to one of the illumination directions. Within each aperture, a phase grating diffracts the light to a separate region on the camera chip, resulting in an image such as that shown in Fig. 1(d).

2.2. 3D coordinate calculation using parallax

The position of a particle within each image is tracked in two dimensions by finding its centre of symmetry [9]. The particle's apparent position is a projection of its 3D position onto the focal plane from a direction defined by the angle of illumination. Figure 2(a) shows how the projected 2D image of a micro-sphere is related to its 3D position. The Cartesian lab. frame in the schematic is defined with the x - y plane parallel to the focal plane. Each illumination direction is defined by azimuthal and polar angles, θ and ϕ respectively. A micro-sphere at position a results in a projected image at location a_i in the focal plane. If the micro-sphere moves vertically up to position b , the corresponding projected image moves to position b_i . If the micro-sphere moves parallel to y (e.g. from position b to c), the corresponding image moves the same distance along the y axis (b_i to c_i), and likewise for motion parallel to the x axis. Therefore it is straight forward to show that for an arbitrary 3D translation of the micro-sphere described by vector $v = [\delta x, \delta y, \delta z]$, its measured motion in the focal plane is described by a 2D vector $v_m = [x_m, y_m]$, where the x -component $x_m = \delta x + \delta z \tan \phi \cos \theta$, and the y -component $y_m = \delta y + \delta z \tan \phi \sin \theta$. The 3 components of v cannot be uniquely identified from a single illumination channel, but can be recovered by combining tracking measurements of the particle from any two arbitrary channels:

$$\delta x = (x_{m_j} \tan \phi_i \cos \theta_i - x_{m_i} \tan \phi_j \cos \theta_j) / (\tan \phi_i \cos \theta_i - \tan \phi_j \cos \theta_j) \quad (1)$$

$$\delta y = (y_{m_j} \tan \phi_i \sin \theta_i - y_{m_i} \tan \phi_j \sin \theta_j) / (\tan \phi_i \sin \theta_i - \tan \phi_j \sin \theta_j) \quad (2)$$

$$\delta z_{from x} = (x_{m_j} - x_{m_i}) / (\tan \phi_j \cos \theta_j - \tan \phi_i \cos \theta_i) \quad (3)$$

$$\delta z_{from y} = (y_{m_j} - y_{m_i}) / (\tan \phi_j \sin \theta_j - \tan \phi_i \sin \theta_i) \quad (4)$$

where the subscripts i, j indicate the channel number ($i \neq j = 1, 2, 3, 4$ in our case), with associated angles θ and ϕ , and components of measured motion, x_m and y_m . δz can be calculated from either the x or y component of the image displacement, as indicated by subscripts in Eqs. (3) and (4). These are chosen or weighted based on their signal to noise ratio, which depends upon the illumination directions relative to the x and y axis. When the azimuthal angles are separated by 180° and aligned with the lab. x -axis (i.e. $\theta_i = 0^\circ$, $\theta_j = 180^\circ$), and the polar angles of the two illuminators are equal, then Eqs. (1)–(3) give those described in [9].

For accurate tracking using Eqs. (1)–(4), the angles of the illumination of each channel must be known. This can be achieved by aligning each channel through an aperture at a preset position in the focal plane. The light is centred on the aperture when the image of a micro-sphere appears most symmetrical. When using an SLM to separate the images, the alignment can also be fine tuned by adjusting the position of the aperture on the hologram. Once the system is aligned in this way, the azimuthal and polar angles of each illumination channel can be calculated from the location of the centre of each aperture on the SLM, without the need for calibration. If necessary, the illumination angles can also be directly measured by monitoring the translation of a micro-sphere fixed to the substrate as it is stepped axially by a known distance.

3. Results

Figures 3(a)–3(c) show a comparison of the two independent measurements of the trajectory of an optically trapped micro-sphere recorded using our four-directional stereo-microscope. The

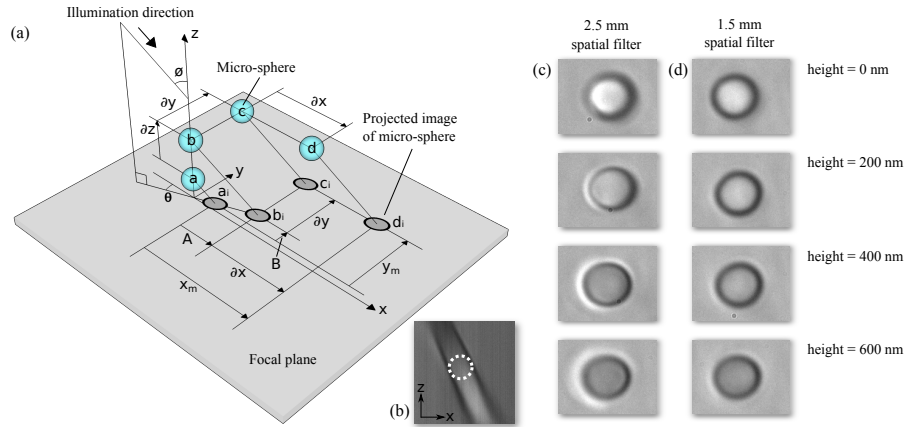


Fig. 2. (a) The relationship between micro-sphere's 3D position to its projected image on the focal plane. The measured motion of the image parallel to x in the focal plane is given by $x_m = A + \delta x$, where $A = \delta z \tan \phi \cos \theta$. Likewise the measured motion of the image parallel to y is given by $y_m = B + \delta y$, where $B = \delta z \tan \phi \sin \theta$. (b) shows a vertical cross-section through a z -stack of images (200 images recorded at 100 nm height separations) of a $5 \mu\text{m}$ diameter micro-sphere illuminated by a single off axis illuminator. The approximate position of the micro-sphere is marked with a dashed white circle. Optimum tracking is achieved by choosing the most symmetrical horizontal plane for centre of symmetry tracking. (c) shows a column of four images of a micro-sphere at different heights with a spatial filter diameter of 2.5 mm. (d) shows the same micro-sphere with a reduced diameter spatial filter. In (d) the images are now more symmetrical, facilitating accurate tracking.

difference between each measurement is shown by the red trace. In this case the azimuthal illumination angles were separated by $\sim 90^\circ$, and the polar angles were all $\sim 25^\circ$. We found no strong dependence of the tracking error with variation in polar illumination angles between $20 - 30^\circ$. The RMS of the differences between each measurement in this case are 2.6 nm in x , 4.5 nm in y and 5.1 nm in z , using data recorded over a 30 s period with an exposure time of $1877 \mu\text{s}$ (corresponding to a frame rate of 532 Hz if not limited by other factors). Figure 3(d) shows a zoom in on part of the axial position trace to more clearly reveal the similarity of the measurements. As shown in Fig. 2, off-axis illumination introduces distortions in the images of a micro-sphere as the horizontal focal plane images at an angle to the illuminating light. These aberrations can be reduced by low-pass spatially filtering the images (the degree of spatial filtering is dictated by the aperture size on the SLM), which removes some of the high spatial frequency distortions. Figure 3(e) shows how the tracking errors depend upon the degree of spatial filtering. If the spatial filter frequency is set too low, the amount of light reaching the camera is significantly reduced, causing the signal to noise ratio to fall, increasing the tracking error. Conversely, if the spatial filter frequency is too high, the distortions in the image of the micro-sphere caused by off-axis illumination change asymmetrically as it moves axially, as shown in Fig. 2(c), which is problematic for the centre of symmetry tracking algorithm, also increasing the tracking error. A balance between these effects results in an optimum tracking error (see Figs. 2(b) and 2(d)). The reduction in the signal to noise ratio due to low light levels is also evident as the light reaching the camera is reduced by shortening the exposure time, as shown in Fig. 3(f). In our set-up the light level was limited by the diffraction efficiency of the SLM, and the 10 nm bandpass filter used to reduce dispersion of light diffracted from the SLM. Despite this, we still find an error of less than 10 nm in each dimension down to

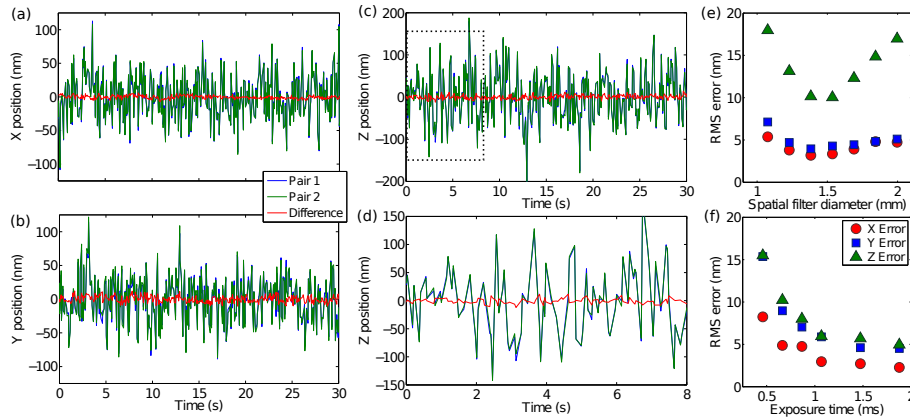


Fig. 3. Accuracy of 3D particle tracking using stereo-microscopy. (a), (b) and (c) show traces of the measured x , y and z positions respectively. In each case the two independent measurements (green and blue lines) are overlaid by subtracting their mean positions. The red trace indicates the difference between the measurements. (d) shows a zoom in on the highlighted region of (c) to more clearly observe the similarity of the measurements. (e) shows how the tracking accuracy in each dimension depends upon the level of spatial filtering. (f) shows how the accuracy depends upon the camera exposure time.

an exposure time of $663 \mu\text{s}$, corresponding to a frame rate of 1508 Hz. This can be further improved by increasing the illumination intensity [21]. Figures 3(e) and 3(f) show a small difference in the minimum error for each dimension. This is representative of the variation in measurements taken with our system, where the measured accuracy was dependent upon system alignment, and the state of the sample (for example, how perfectly spherical and optically clear the micro-sphere of interest was). Throughout our measurements we obtained accuracies of 2-5 nm laterally, and 5-10 nm axially on a $5 \mu\text{m}$ diameter optically trapped micro-sphere.

4. Conclusion

Submerged microscopic particles undergo stochastic thermal motion, resulting in a tracking signal that is inherently difficult to separate from random noise. In this work, we have shown how an SLM microscope can be used to provide a real-time evaluation of the 3D particle tracking accuracy in high-speed video stereo-microscopy. We have demonstrated an accuracy of less than 2.5% of the range of motion of a $5 \mu\text{m}$ diameter optically trapped micro-sphere, and shown how the error depends upon the degree of spatial filtering, and camera exposure time, allowing us to optimise the system. Knowledge of this error can also be factored into the stiffness calibration of optical tweezers for accurate force measurements, and used to more accurately recover micro-rheological properties of a sample. As the error signal is generated in real-time, it can also be used to alert an operator during an experiment if an unwanted piece of detritus is attracted into an optical trap.

Acknowledgments

This work was supported by the EPSRC (grant number EP/I007822/1). MJP acknowledges support from the Royal Society. We would like to thank Richard Bowman for useful discussions.